LA-UR-16-20116
Approved for public release; distribution is unlimited.

Title: Shock Detector for SURF model

Author(s): Menikoff, Ralph

Intended for: Report

Issued: 2016-01-11

Shock Detector for SURF model

Ralph Menikoff

December 22, 2015

Abstract

SURF and its extension SURFplus are reactive burn models aimed at shock initiation and propagation of detonation waves in high explosives. A distinctive feature of these models is that the burn rate depends on the lead shock pressure. A key part of the models is an algorithm to detect the lead shock. Typically, shock capturing hydro algorithms have small oscillations behind a shock. Here we investigate how well the shock detection algorithm works for a nearly steady propagating detonation wave in one-dimension using the Eulerian `xRage` code.

1 Introduction

The SURF model and its extension SURFplus [Shaw and Menikoff, 2010, Menikoff and Shaw, 2010] are reactive burn models aimed at shock initiation and propagation of detonation wave in high explosive (HE). SURF is based on the ignition and growth concept of hot spots in a heterogeneous HE [Lee and Tarver, 1980]. SURFplus adds a second reaction for the energy release as excess carbon bonds to form clusters that grow in size to nanometer particles of diamond or graphite.

Key assumptions of the hot-spot model are that the burn rate scales with the average distance between hot spots, and that the number density of hot spots is determined by the lead shock pressure. The dependence of the burn rate on the lead shock pressure naturally accounts for shock desensitization. In contrast, most burn models base the burn rate on only the local hydrodynamic variable, most strongly on the pressure and a depletion factor that vanishes when the reactants are all burned.

The SURF model includes an algorithm for detecting the lead shock based on the Hugoniot equation for the energy; see appendices A and B. The detection algorithm is local (*i.e.*, cell by cell), and depends only on thermodynamic variables (pressure, specific energy and specific volume). Being independent of velocity, in principle, the detection algorithm does not depend on the direction of shock propagation.

SURF is intended to be implemented in hydro codes that utilize shock capturing algorithms. Typically, small oscillations occur behind a shock. Moreover, the numerical shock width is always a few cells, and the amplitude of the oscillations does not diminish with finer mesh resolution. This raises the questions of how well the shock detector works, and whether numerical fluctuations in the detected shock pressure would affect the stability of the model for propagating a detonation wave.

Here we investigate these questions for a promptly initiated and nearly steady one-dimension detonation wave with both the SURF and SURFplus models. For this purpose, we use the Eulerian `xRage` code and HE parameters corresponding to PBX 9502; see appendices C and D.

For the original implementation of the SURF model, a cell did not start burning until after the shock is detected. When the reaction profile is not resolved (coarse resolution), this has the advantage of better capturing the von Neumann (VN) spike or lead shock in the Zel'dorvich-von Neumann-Doering (ZND) detonation wave profile [see Fickett and Davis, 1979, § 2C]. However, a side effect is that it leads to oscillations in the arrival time of the detected shock. This affects when a cell starts burning and causes pressure fluctuations that exacerbate the ability of the shock detector to determine when the shock profile ends in the next cell.

Three implementation changes can reduce the fluctuation in the shock pressure:
i. Smoothing the shock pressure by averaging the value in neighboring cells. This is effective for short wavelength spatial oscillation; *i.e.*, every other cell.
ii. Reducing the CFL number. This results in more time steps for the shock rise time within a cell. Hence, a better resolved Hugoniot function time history that is used in the detection algorithm to determine when the shock profile ends. Unfortunately, this is inefficient as it increases the number of cycles needed for a simulation.
iii. Allowing burning to take place in the shock profile above a threshold pressure. This is the most effective. However, it does lower the VN-spike pressure for a propagating detonation wave. The small decrease in the shock pressure can be accounted for in the calibration of the burn rate.

As will be seen in the simulations in the following sections, small oscillations in the shock pressure do not affect the overall stability of a propagating detonation wave.

2 Test problem

As a test problem we use a propagating 1-D detonation wave with model parameters corresponding to PBX 9502; Davis EOS for reactants and products with parameters in Appendix C, and SURF and SURFplus burn model parameters in Appendix D.

The detonation wave is initiated promptly by a small (0.5 mm) 'hot-spot' region adjacent to the left boundary. The boundary is a rigid wall and the hot spot consists of the products at the Chapman-Jouguet (CJ) state with a linear velocity from 0 at the wall to the CJ particle velocity at the interface with the reactants. The hot-spot pressure generates a strong shock in the reactants which leads to a prompt (within a few mm) shock-to-detonation transition.

After the transition to a detonation, the flow approaches a steady CJ-detonation wave followed by a rarefaction or Taylor wave. The rarefaction extends from the detonation state to a particle velocity of 0 in order to meet the boundary condition set by the wall. The approach to a steady detonation is more rapid for the SURF model (fast hot-spot reaction) then for the SURFplus model (SURF model plus relatively slow carbon-clustering reaction).

The width of the reaction zone is about 0.2 mm for the SURF model and about 2.7 mm for the SURFplus model. The mesh allows the detonation wave to propagate 100 mm; roughly 500 and 35 reaction zone lengths for the SURF and SURFplus models, respectively. This is long enough to check for numerical instabilities or anomalies in propagating a detonation wave.

The `xRage` code treats partly burned HE as a mixed cell of reactants and products in P-T equilibrium. A P-T table for each component is used to evaluate the equilibrium EOS. To minimize interpolation errors we use a very fine table; 120 points per decade in pressure and 40 points

per decade in temperature. For pure cells (all reactants or all products) the `use_direct=true` option is used to evaluate the analytic formulas for the Davis EOS. This gives an accurate pressure needed to calculate the spreading of the rarefaction wave.

The `xRage` code has an adaptive mesh refinement capability. Detonation wave simulations typically use a mesh with an initial cell size on the order of 1 mm and then refine regions with a high pressure gradient and the reaction zone of an HE. Here, to avoid issues with refining and coarsening the mesh, we use a uniform grid with a cell size of 0.01 mm. This is small compared to the fast-reaction zone width of about 0.2 mm.

A time step of $\Delta t = 0.27\Delta x/D_{cj}$ is used. It is chosen not to be an integer multiple of the transit time of the detonation wave across a cell. This avoids a periodicity in time of the discretization of the reaction zone, which avoids constructive or destructive interference that would affect fluctuations of the detected shock pressure. We note that there will be roughly 4 times as many time steps in the shock rise as the number of cells in the shock profile.

The cell variables for the shock pressure and shock arrival time are advected. To better evaluate the shock detector, a diagnostic output has been added that prints out the cell location, the shock pressure and the shock arrival time as the lead shock is detected. The shock speed is calculated from the shock arrival time. In addition, time histories at a fixed cell location (Eulerian tracer particles at $x = 50$, 70 and 90 mm) are used as a check on the shock profile and the Hugoniot function upon which the shock detector is based.

3 SURF simulations

For the first simulation, a pressure threshold for burning, `Pburn` = 40 GPa, slighly lower than the VN-spike pressure is used; see Eq. (B.1). The shock detector pressure is shown in fig. 1. Adjacent pairs of points have been averaged to reduce short wavelength fluctuations. The detected shock pressure is close to the VN-spike pressure and the amplitude of the fluctuations are small; about $\pm 0.06\,\%$.

The shock speed derived from shock detector arrival time is shown in fig. 2. The shock speed is smoothed by taking the slope of a linear fit to $x(t)$ over 1 mm intervals. The smoothed shock speed is close to the CJ-detonation speed and the fluctuations are small. With a smaller smoothing distance the fluctuation would be much larger.

Tracer particle time histories of the shock pressure and the Hugoniot function are shown in fig. 3. There is a slight jitter in the time dependence due to the discretization of shock profile and the pressure threshold for burning. More important is that the Hugoniot function crosses 0

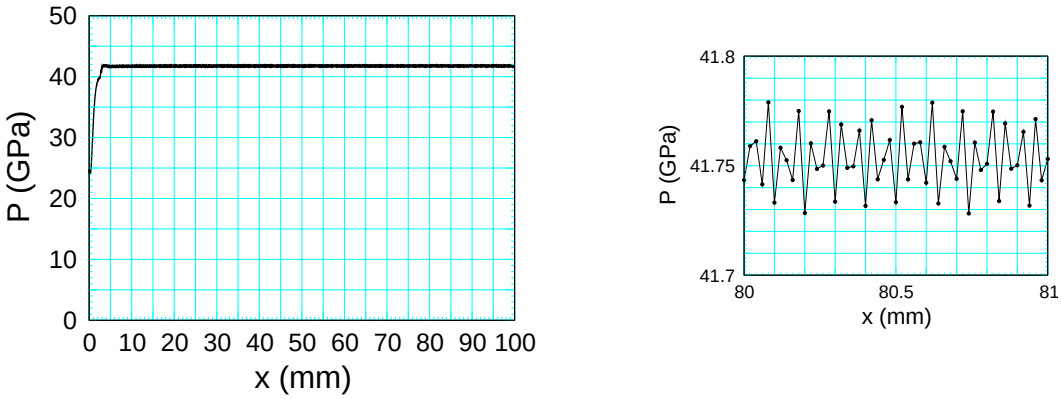

Figure 1: Shock pressure vs distance for SURF model simulation. Zoomed plot shows the pressure fluctuations. Symbols correspond to cells.

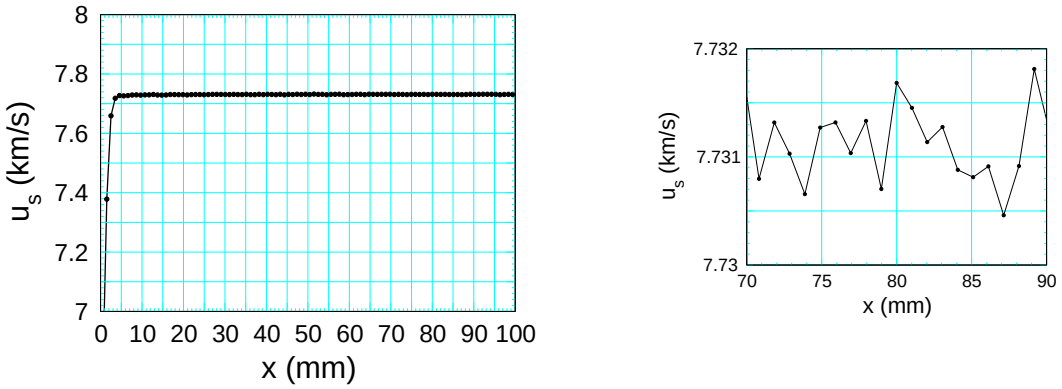

Figure 2: Shock speed vs distance for SURF model simulation. Zoomed plot shows the fluctuations in the shock speed. Shock speed is smoothed over an interval of 1 mm.

tangentially rather than transversally. This leads to some jitter in the detected shock pressure and shock arrival time.

Pressure and reaction progress variable versus V are shown in fig. 4. Key features, in accord with theory, are that the shock profile lies just above the shock locus, and the pressure in the reaction zone is along the Rayleigh line. The zoomed plot shows the end of shock profile and the beginning of reaction zone. With `Pburn` set to 40 GPa there is 1 to 2 % burning at the end of the shock profile, and the detected shock pressure is a little lower than the VN-spike pressure. We also note that the detected shock pressure is slightly below the peak pressure.

Spatial pressure profiles for a sequence of times are shown in fig. 5. The zoomed plot shows that the reaction-zone profiles overlap. Consequently, the detonation wave is steady and hence stable. As expected the slope of the Taylor wave decreases with time.

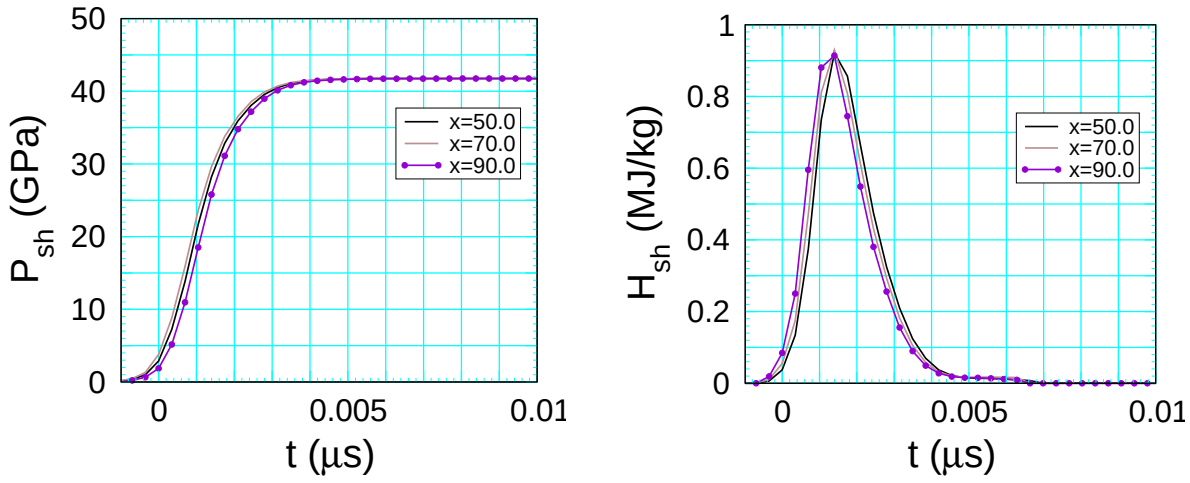

Figure 3: Shock pressure and Hugoniot function at 3 tracer points for SURF model simulation. Time origins have been shifted to the beginning of the profile. The symbols on the last tracer correspond to time steps.

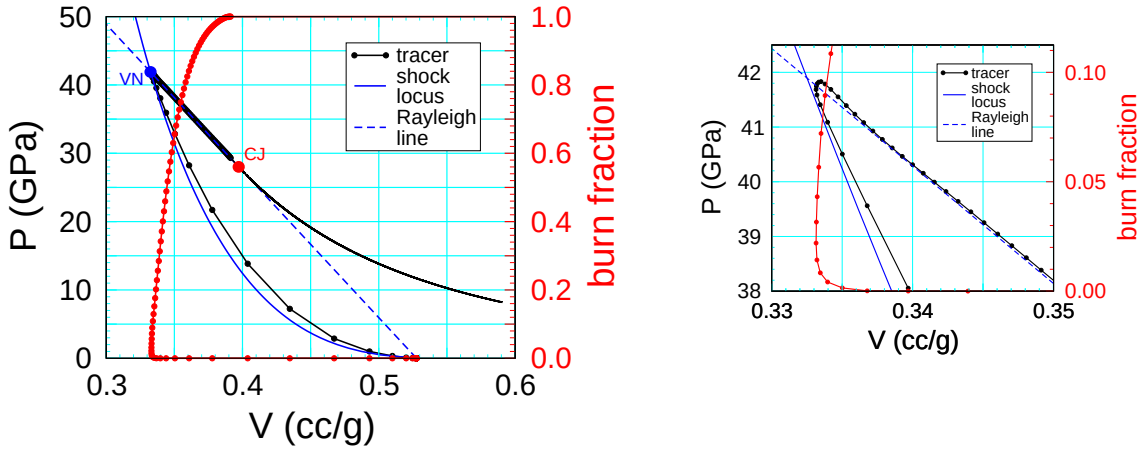

Figure 4: Trajectories in (V, P)-plane and (V, λ)-plane from time history at fixed position for SURF model simulation. Also shown are the shock locus, and the Rayleigh line for the CJ detonation. Symbols correspond to time steps for the shock profile and reaction zone.

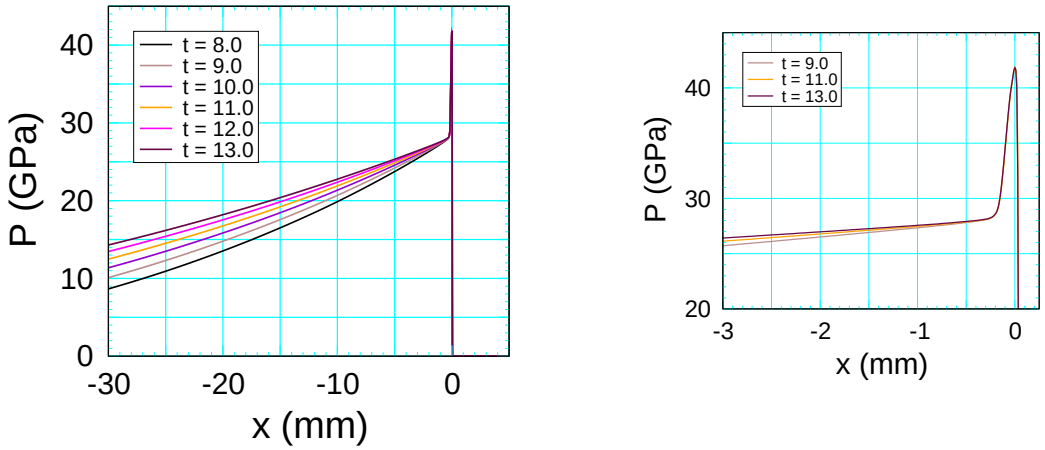

Figure 5: Pressure profiles at sequence of times for SURF model simulation. Detonation front has been shifted to the origin.

3.1 No reaction in shock profile

A simulation with `Pburn` $> P_{VN}$, illustrates the effect of jitter in the shock arrival time when the reaction starts after the shock is detector. Figure 6 shows the variation in the shock pressure and Hugoniot function for the 3 tracer particles. The variation in the tail of the Hugoniot profile,

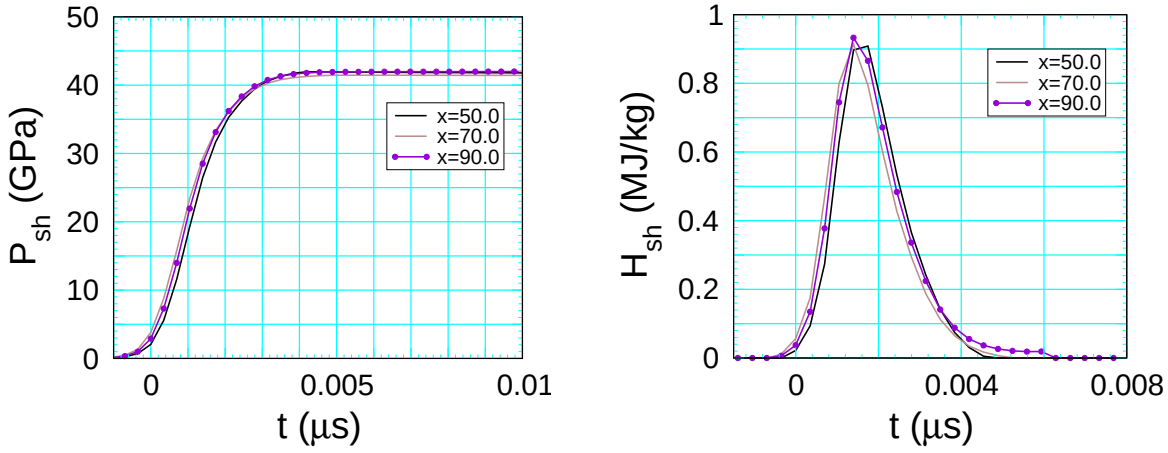

Figure 6: Shock pressure and Hugoniot function at 3 tracer points for SURF model simulation with no reaction in shock profile. Time origins have been shifted to the beginning of the profile. The symbols on the last tracer correspond to time steps.

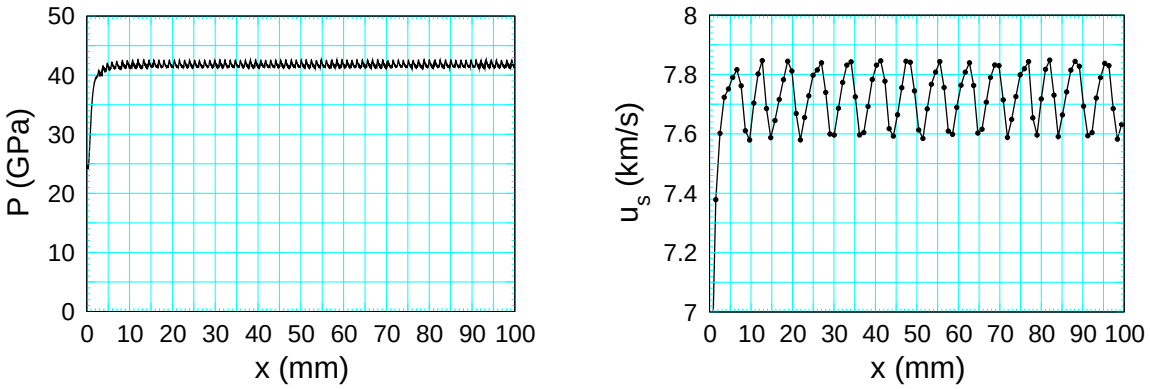

Figure 7: Shock pressure and smoothed shock speed vs distance for SURF model simulation with no reaction in shock profile.

due to feed back with the reaction, is critical for determining the shock arrival time. As seen in fig. 7, this result in significant oscillations in both the shock pressure and the smoothed shock speed. The wavelength of the oscillation is several mm, which is much longer than the reaction zone width.

A sequence of pressure profiles is shown in fig. 8. While the reaction zone is nearly steady, acoustic waves are radiated back into the Taylor wave and give rise to small but observable pressure fluctuations.

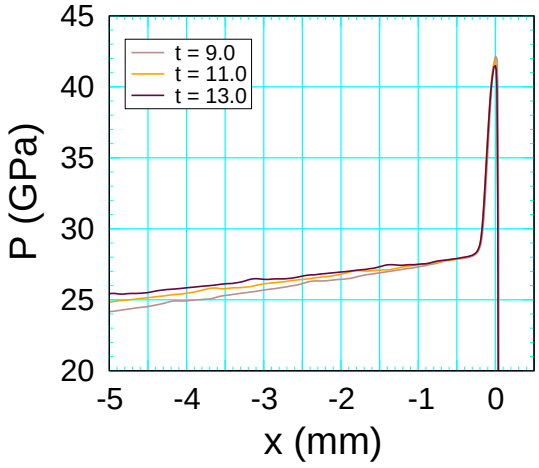

Figure 8: Pressure profile at sequence of times for SURF model simulation with no reaction in shock profile. Detonation front has been shifted to the origin.

4 SURFplus simulation

Compared to the SURF model, the additional slow reaction in the SURFplus model results in qualitatively differences in important detonation wave properties. First, the CJ detonation wave profile is much wider; see fig. 9. However, the CJ state, which depends on the products EOS, is the same for the SURF and SURFplus models. The state at the end of the hot-spot reaction (SURF rate) is different. For the SURFplus model, it is determined by the detonation locus of the products with the carbon-clustering energy subtracted out; see Eq. (B.4) and fig. 26 in the appendix.

In two and three dimensions, important consequences of increasing the reaction-zone width are that the curvature effect increases (*i.e.*, for given front curvature $\kappa > 0$, $D_{\rm CJ} - D_n(\kappa)$ increases, or the detonation speed $D_n(\kappa)$ decreases) and the failure diameter increases (*i.e.*, the threshold diameter of a rate stick below which a detonation wave fails to propagate).

The second slow reaction of the SURFplus model also affects shock initiation and the approach of the detonation wave to steady state. Due to the disparity in the hot-spot and carbon-clustering reaction times, prompt initiation leads to a detonation wave at the CJ state on the detonation locus without the carbon-clustering energy. As seen in fig. 26, both the pressure and the detonation speed are lower than that at the CJ state of the full fast-slow reaction. Subsequently, as will be seen in the next simulation, the detonation speed and lead shock pressure buildup to the values of the CJ detonation wave of the full reaction.

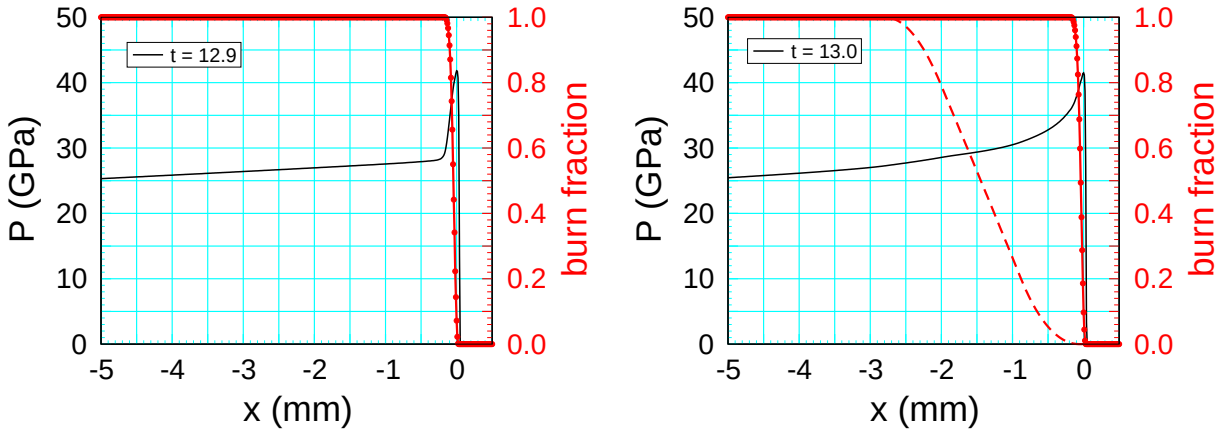

Figure 9: Shock pressure and reaction progress variables vs distance for SURF and SURFplus models, left and right plots, respectively. Symbols on the hot-spot reaction progress variable (solid red line) correspond to cells. Dashed red line is the second or carbon-clustering reaction progress variable.

For the SURFplus simulation, the CJ pressure is used for the threshold burn pressure, `Pburn`. The shock detector pressure is shown in fig. 10. Again adjacent pairs of points are averaged to reduce short wavelength fluctuations. The shock speed derived from the shock detector arrival time is shown in fig. 11. Again the shock speed is smoothed by taking the slope of a linear fit to $x(t)$ over 1 mm intervals.

Compared to the corresponding plots for the SURF model, fig. 1 and fig. 2, prompt initiation after 3 to 4 mm leads to a lower shock pressure and a lower detonation speed. The lower values correspond to the detonation locus without the carbon clustering energy; see tables 2 and 3 in the appendix. Subsequently the lead shock pressure and the detonation speed increase and approach the values for the CJ state of the detonation locus with the carbon clustering energy. The fluctuation in the pressure and speed are comparable for the two models.

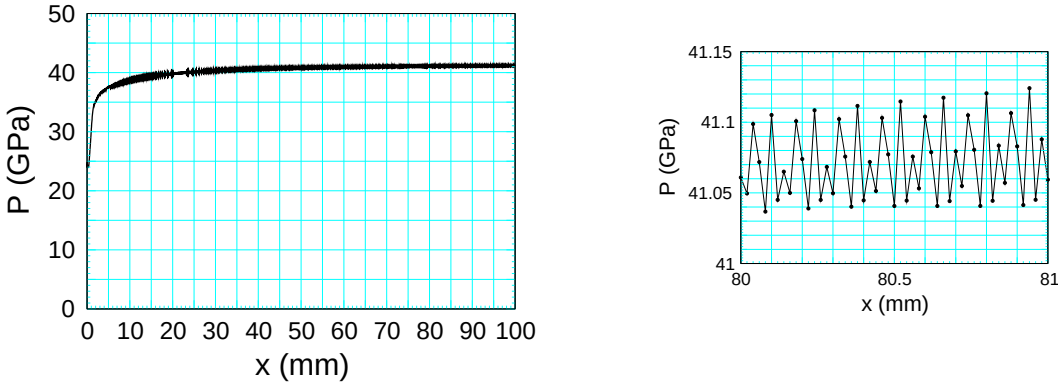

Figure 10: Shock pressure vs distance for SURFplus model simulation. Zoomed plot shows the pressure fluctuations.

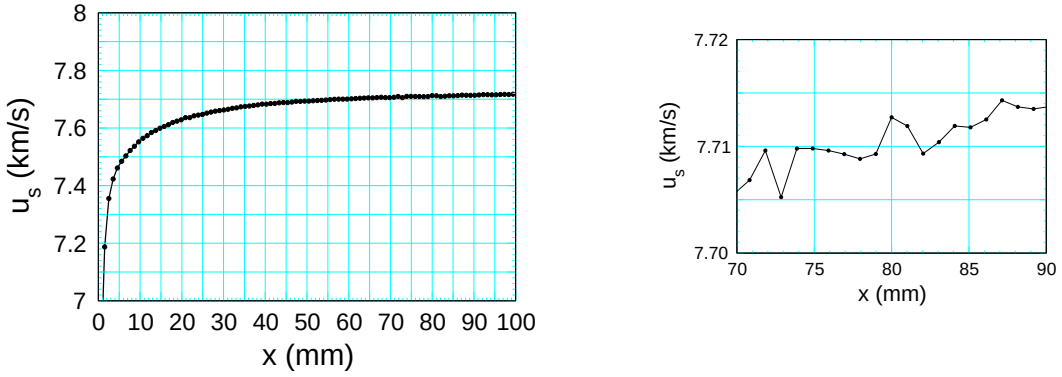

Figure 11: Smoothed shock speed vs distance for SURFplus model simulation. Zoomed plot shows the fluctuations in the smoothed shock speed.

Tracer particle time histories of the shock pressure and the Hugoniot function are shown in fig. 12. Compared to the plots for the SURF model, fig. 3, the jitter is slightly less. This may be due to the lower value used for the pressure threshold, `Pburn`, or the neighborhood of the sonic point being better resolved due to the slower rate at the end of the reaction zone.

The pressure and reaction progress variables versus V are shown in fig. 13. Due to the slow approach to the steady CJ detonation wave, the second carbon clustering reaction ends at a

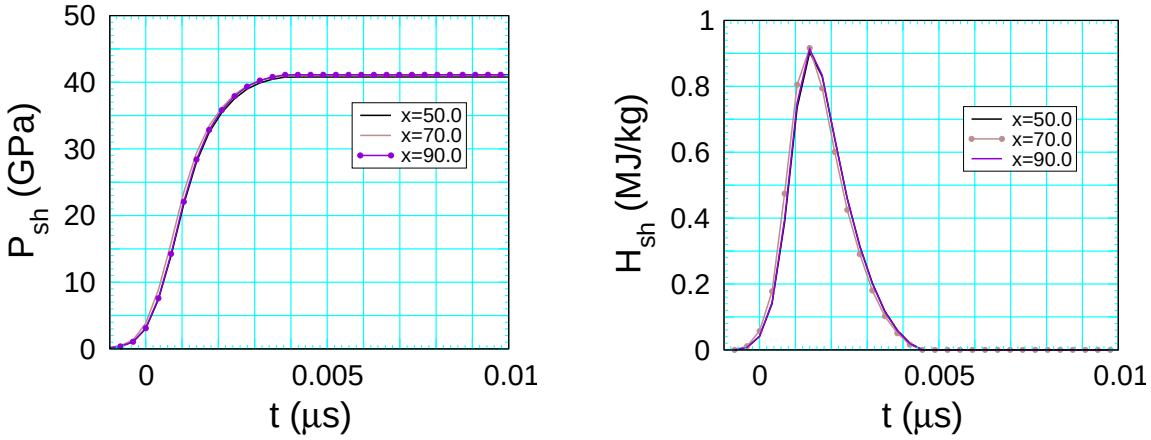

Figure 12: Shock pressure and Hugoniot function at 3 tracer points for SURFplus model simulation. Time origins have been shifted to the beginning of the profile. The symbols on the last tracer correspond to time steps.

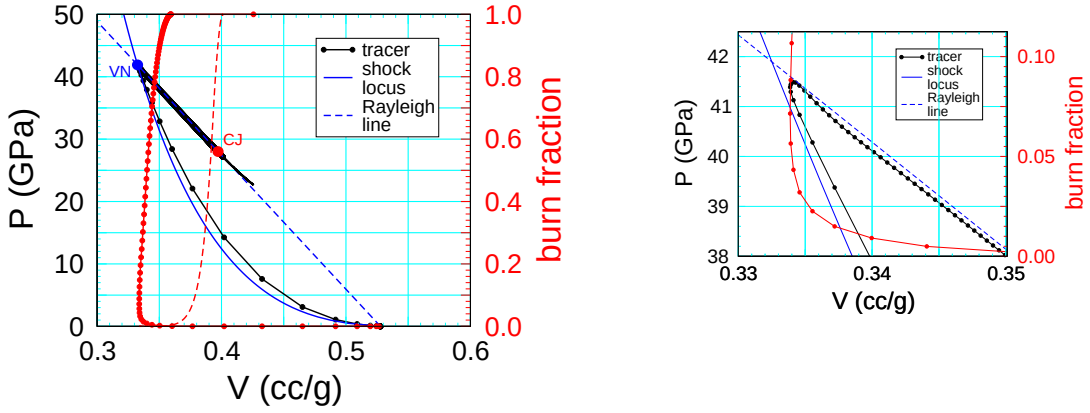

Figure 13: Trajectories in (V, P)-plane and (V, λ)-plane from time history at fixed position for SURFplus model simulation. Also shown are the shock locus, and the Rayleigh line for the CJ detonation. Symbols correspond to time steps for the shock profile and reaction zone.

slightly lower pressure than that of the CJ state. The SURF reaction ends at a higher pressure since the carbon clustering energy has not yet been released. The zoomed plot shows about 4% hot spot reaction at the end of the shock profile. The increased amount is due to the lower pressure threshold for the start of burning. The burning towards the end of the shock profile lowers the peak pressure and consequently the detected shock pressure.

Spatial pressure profiles for a sequence of times are shown in fig. 14. The zoomed plot shows that the reaction zone profiles nearly overlap. Due to the slow approach to the steady CJ detonation wave seen in fig. 10 and fig. 11, the overlap does not extend down to the CJ pressure.

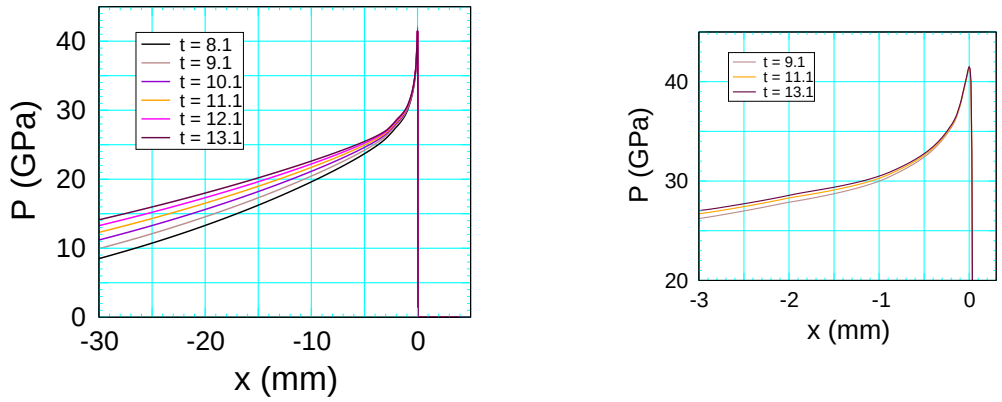

Figure 14: Pressure profiles at sequence of times for SURFplus model simulation. Detonation front has been shifted to the origin.

5 Comparison model simulation

For comparison, the next simulation uses the same EOS and grid but a burn rate depending on the local pressure rather than the shock pressure. In this case, the shock detector is a passive diagnostic that is not used in the simulation. It is meant as a check on whether removing the coupling between the detected shock pressure and the reaction would significantly decrease the oscillations in the shock pressure.

For this purpose, the WSD model with 9502 parameters from Wescott et al. [2005] is used. The WSD model has a single reaction with fast and slow rates. The rate is smoothly switched based on the reaction progress variable; fast rate for $0 \leq \lambda \lesssim \lambda_c$, and slow rate for $\lambda_c \lesssim \lambda \leq 1$ where for 9502 $\lambda_c = 0.9$. This has an effect similar to the SURFplus model, with the fast and slow rates corresponding to the first (hot spot) and second (carbon clustering) reactions, respectively.

The shock detector pressure is shown in fig. 15. Again adjacent pairs of points are averaged to reduce short wavelength fluctuations. The smoothed shock speed derived from the shock detector arrival time is shown in fig. 16. Analogous to the SURFplus, these plots show a prompt initiation, due to the fast reaction, followed by a slow increase in shock pressure and shock speed approaching the values for a CJ detonation wave. Moreover, the zoomed plots show the fluctuation are comparable.

Tracer particle time histories of the shock pressure and the Hugoniot function are shown in fig. 17. The shock is detected at the pressure peak since the pressure decreases before the Hugoniot function goes to 0. The WSD profiles show a little more jitter than those of the SURFplus model.

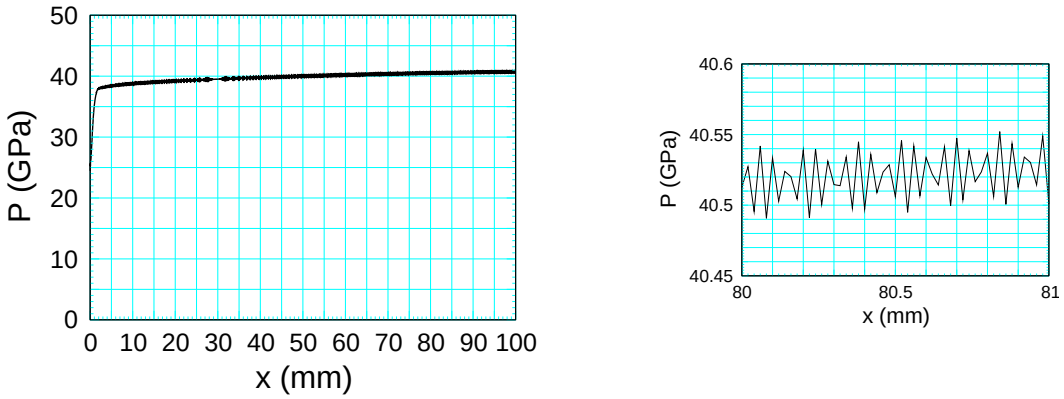

Figure 15: Shock pressure vs distance for WSD model simulation. Zoomed plot shows the pressure fluctuations.

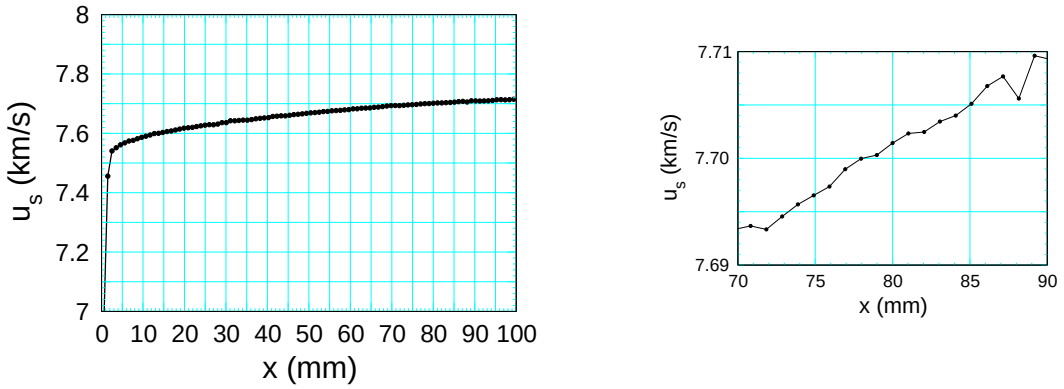

Figure 16: Smoothed shock speed vs distance for WSD model simulation. Zoomed plot shows the fluctuations in the smoothed shock speed.

The pressure and reaction progress variable versus V are shown in fig. 18. The zoomed plot shows more reaction in the shock profile and a peak pressure further below the VN-spike than the SURFplus model. This is more apparent in fig. 19 which shows the reaction progress variables versus pressure for both the SURFplus and WSD simulations. The low amount of burning in the shock profile for the SURF model is partly due to the rate being 0 at the shock front; see Eq. (D.3) and fig. 23. The plot also shows the correspondence between the two SURFplus

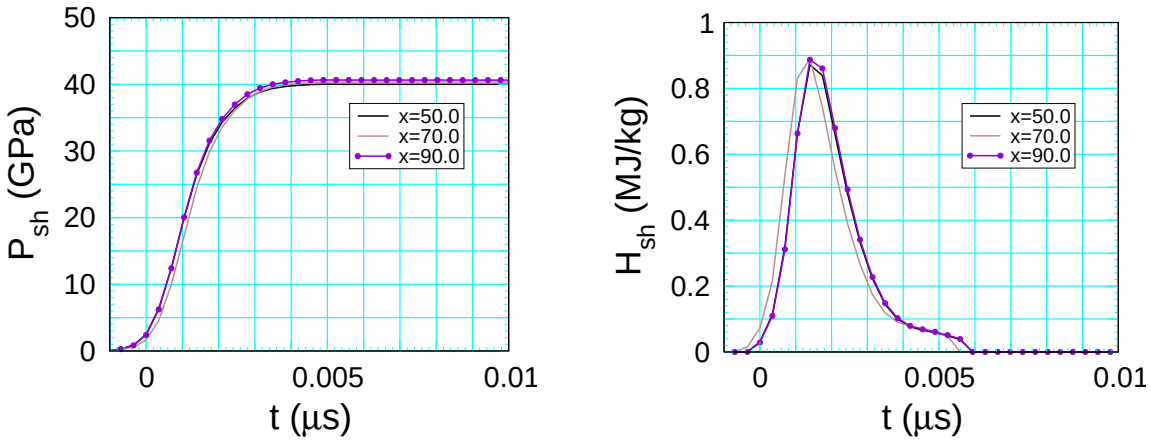

Figure 17: Shock pressure and Hugoniot function at 3 tracer points for WSD model simulation. Time origins have been shifted to the beginning of the profile. The symbols on the last tracer correspond to time steps.

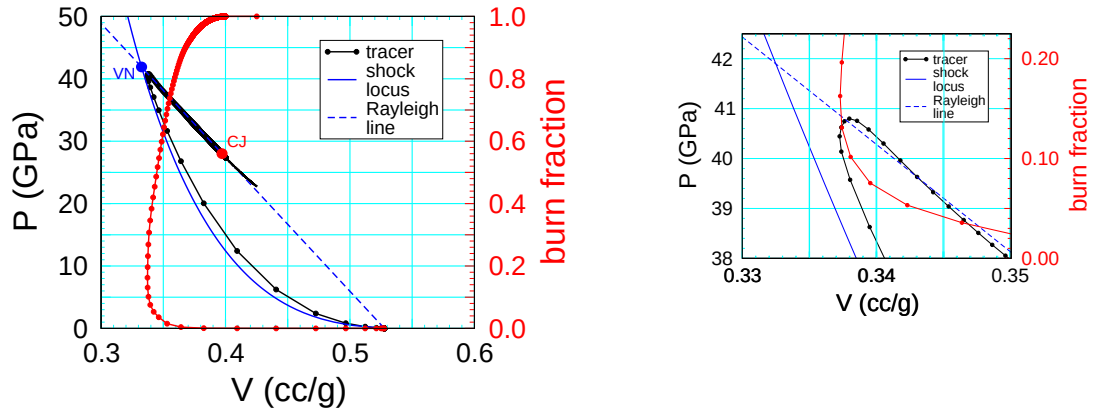

Figure 18: Trajectories in (V, P)-plane and (V, λ)-plane from time history at fixed position for WSD model simulation. Also shown are the shock locus, and the Rayleigh line for the CJ detonation. Symbols correspond to time steps for the shock profile and reaction zone.

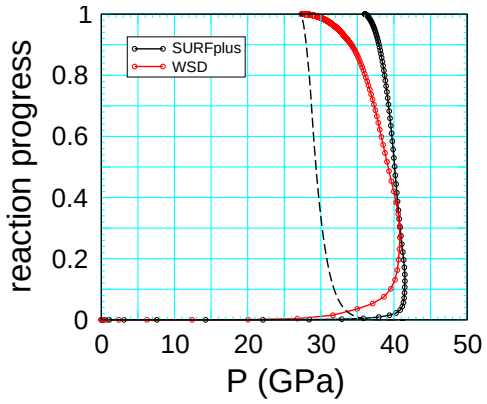

Figure 19: Trajectories of reaction progress variables vs pressure from time history at fixed position for SURFplus model simulation (solid first reaction and dashed second reaction) and WSD model simulation. Symbols correspond to time steps for the shock profile and reaction zone.

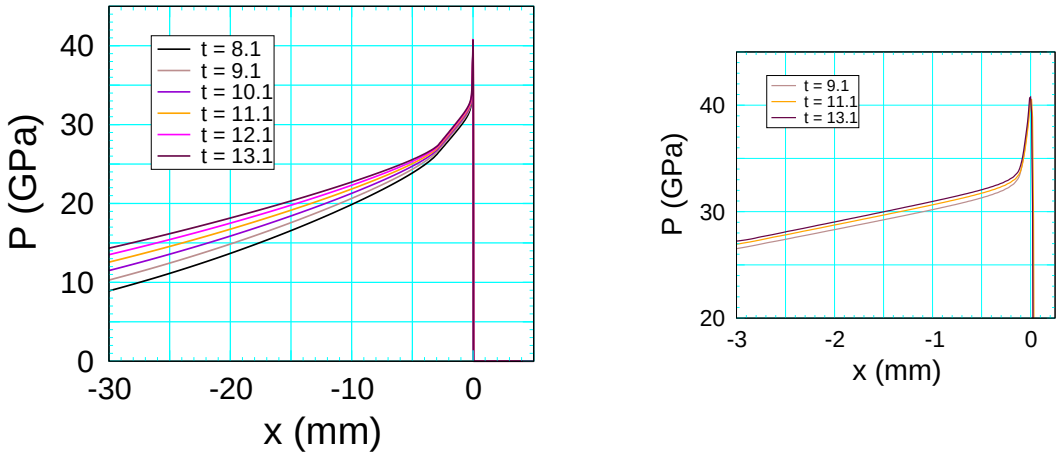

Figure 20: Pressure profiles at sequence of times for WSD model simulation. Detonation front has been shifted to the origin.

reactions and the single WSD reaction; *i.e.*, the second SURFplus reaction correspons to the last 10 to 15% burning of the WSD model.

Spatial pressure profiles for a sequence of times are shown in fig. 20. The fast reaction gives rise to a pressure spike followed by a lower slope for slow reaction and then the Taylor wave. The zoomed plot shows that the reaction zone profiles for the fast reaction nearly overlap. The reaction profile for the slow rate, down to $P_{\mathrm{CJ}} = 28\,\mathrm{GPa}$ has not reached steady state.

Overall the WSD and the SURFplus simulations show very similar behavior for initiation and propagation of the detonation wave. There is no evidence that the coupling of SURF burn rate to the fluctuations in the detected shock pressure is adversely affecting the reaction zone.

6 Summary

Simulations with the `xRage` code show fluctuation in the detected shock pressure used in the SURF model rate. The threshold burn pressure, `Pburn` in Eq. (B.1b), that allows up to a few per cent burning at the end of the shock profile can reduce the oscillation to about 0.1%. Since the derivative of the rate, $\mathtt{d} \ln Rate(P_s)/\mathtt{d}P_s$ is small for $P_s > P_{\mathrm{CJ}}$, see fig. 22, the fractional change in the rate from oscillations in P_s is reduced from the relative error in P_s. Simulations show that the effect on the reaction zone profile is small, and does not affect the stability of a propagating detonation wave.

Burning in the shock profile does lower the peak pressure and consequently lowers the detected shock pressure. This can likely be compensated for in the calibration of the rate. Since the numerical dissipation used for shock capturing varies with hydro code, there can be variations on the detected shock pressure that also may require slight adjustments of the rate parameters.

In principle fluctuations in the detected shock pressure can be decreased by using a finer resolution and averaging the shock pressure over a number of cells. As long as the shock transit time over the averaging distance is small compared to the reaction time, the averaging should not have adverse side effects. Ideally, adaptive mesh refinement could be used in the neighborhood of the shock front. This would minimize the expense of the finer grid, provided that the time step varies on each refinement level with the cell size on that level. Unfortunately, the `xRage` code uses the same time step on all levels, and the finest level determines the time step.

Even without burning, shock capturing algorithms display small post-shock oscillations. Other simulations indicate post shock oscillation decrease with a smaller time step. We conjecture that this can be explained as follows. Due to discretization to a grid, the three jump conditions are not satisfied at exactly the same time. The post-shock oscillations result from equilibrating the conserved quantities to the shock state. Since shock capturing aims to have only a few cells in the shock profile, large truncation errors exacerbate the time variation in when each jump condition is satisfied. Having more time steps within the profile would decrease the truncation errors and allow the jump conditions to be more nearly satisfied simultaneous. Consequently, a smaller time step can help reduce the amplitude of fluctuations in the shock detector pressure.

Two steps are planned to further test the SURF model implementation. First is to check the shock detector for mesh orientation effects with simulations in two-dimensions. Second is

a quantitative comparison with an accurate solution of the ZND profile with following Taylor wave obtained from solving ODEs [see for example, Menikoff, 2015]. We anticipate that the accuracy would be limited by the fluctuations in the shock detector pressure and burning that occurs in the shock profile.

APPENDICES

A Shock detection algorithm

The algorithm for detecting the lead shock is based on the Hugoniot function. It requires three grid variables: Hugoniot function, H; shock pressure, P_s; and shock arrival time t_s. It also needs three variables for the initial state; P_0, V_0, e_0. To account for mixed cells in an Eulerian code, this may require additional grid variables. The shock detector has three states:

	state	condition
1	ahead of shock	$H = P_s = t_s = 0$
2	inside shock profile	$H, P_s, t_s > 0$
3	wave detected	$H = 0$, $t_s > 0$
	A. shock wave	$P_s > 0$
	B. compressive wave or thermal hot spot	$P_s = 0$

The following notation is used for code variables.

```
! time: cycle time
! Pmin: threshold pressure to start shock detection algorithm
!       default 0.1 GPa
! nprofile: max number of cells in shock profile
!       default 10
! ***** cell variables *****
! Ps, ts, H:  shock pressure, arrival time, Hugoniot function
! P0, V0, e0: initial pressure, specific volume, specific energy
! P1, V1, e1: current pressure, specific volume, specific energy
```

Fortran-style pseudo code (without cell indices) for the shock detection algorithm is as follows:

```
loop ! over all grid cells
  if( H.eq.0.0 .and. ts.gt.0.0 )    cycle  ! shock detected
  if( H.eq.0.0 .and. P1.lt.Pmin )   cycle  ! below threshold

  H1 = e1-e0 - 0.5*(P1+P0)*(V0-V1)         ! Hugoniot function
  if( H .eq. 0.0 ) then
      if( H1.gt.0.0 .and. V1.lt.V0 ) then
          Ps = P1
          ts = time
          H  = H1    ! start detection algorithm
      else
          ts = time  ! compressive wave detected
      endif

  else if( H1 .le. 0.0 ) then ! shock followed by compression wave
      Ps = P1
      ts = time
      H  = 0.0       ! shock state set

  else if( P1.le.Ps ) then    ! shock followed by rarefaction
      ts = time
      H  = 0.0       ! shock state set

  else
      us = V0*sqrt( (P1-P0)/(V0 - V1) )         ! shock wave speed
      if( time-ts .gt. nprofile*dx/us ) then    ! time out
          ! shock profile too spread out
          ! weak shock or overly dissipative wave interaction
          Ps = P1
          ts = time
          H  = 0.0  ! shock state set
      else ! inside shock profile
          Ps = P1
          H  = H1
      endif

  endif
```

Reaction source terms in hydro codes are usually accounted for with an operator split methodology. In this sense, the shock detection algorithm can be thought of as evaluating source terms for the additional variables Ps, ts and H; that is, the hydro equations are augmented with variables evolving by rate-like equations;

$$\frac{\mathsf{d}}{\mathsf{d}t}\begin{pmatrix} Ps \\ ts \\ H \end{pmatrix} = \text{source terms} \ , \tag{A.1}$$

where $\mathsf{d}/\mathsf{d}t = \partial_t + u\,\partial_x$ is the convective time derivative.

For an Eulerian code, the shock detection grid variables need to be advected. Since the shock detection algorithm depends on the state of the detector, advection of the shock detector variables should only be applied to cells for which the shock has been detected; *i.e.*, $H = 0$ and $ts > 0$. We note that the shock detector variables are not conserved quantities, so modifying their advection does not cause mathematical difficulties. The advection caveat does not apply to the initial state variables P0, V0 and e0. Advecting these variables is needed to detect the lead shock at mixed-cell material interfaces.

B SURF burn model

The SURF model is expressed in terms of a scaled reaction variable s. The reaction progress variable (mass fraction of products), λ, is determined by the equations

$$\lambda = g(s) \ , \tag{B.1a}$$

$$\mathsf{d}s/\mathsf{d}t = \begin{cases} \Big[\max(0, \min(1, P/P_s))\Big]^n f(P_s) & \text{shock detected or } P_s > P_{burn} \\ 0 & \text{otherwise} \end{cases} \tag{B.1b}$$

where P_s and P are the lead shock pressure and the local pressure, respectively.

A specific HE is characterized by two functions: the reaction scale function $g(s)$ and the reaction strength function $f(P_s)$. The $(P/P_s)^n$ term is needed to fit failure diameter data. Activated only in expansion, this term has minimal effect on a shock-to-detonation transition driven by a sustained shock. It does affect the transition when the driving shock is followed by a rarefaction.

The SURF rate equation (B.1b) is activated after the lead shock is detected or when `Ps > Pburn`. With the parameter `Pburn` greater than the von Neumann spike pressure, burning would

not occur until after the shock is detected. Consequently, the shock detection algorithm would not affect shock capturing aspects of the hydro algorithm. However, the shock detector may give oscillations in P_s. A smaller value for `Pburn` decreases the oscillations. But a side-effect is that the von Neumann spike of the ZND detonation wave profile would be slightly clipped. Clipping of the von Neumann spike also occurs for typical reactive models for which the burn rate depends on pressure, and can be severe when the reaction zone is not sufficiently resolved. In either case, burning in the shock profile is minimized by decreasing the cell size, which reduces the shock rise time relative to the burn time.

The fitting forms used for the reaction strength function and the reaction scale function are given in the appendix D, along with an illustrative example of parameters corresponding to PBX 9502.

B.1 SURFplus extension

The SURFplus model adds a second reaction progress variable, λ_2, to account for the energy release from carbon clustering. The carbon cluster energy is given by

$$e_{CC}(\lambda_2) = \left(\Big[\lambda_2 \, N_{\text{ratio}} + (1 - \lambda_2) \Big]^{-1/3} - N_{\text{ratio}}^{-1/3} \right) Q \ , \tag{B.2}$$

where Q and N_{ratio} are model parameters with dimensions of specific energy and dimensionless, respectively. The rate equation for λ_2 is

$$\mathsf{d}\lambda_2/\mathsf{d}t = \lambda^2 h'\Big(h^{-1}(\lambda_2)\Big) \ , \tag{B.3}$$

where $h(t)$ is a model function for the limiting time dependence of λ_2 in a steady CJ detonation wave, $h' = \mathsf{d}h/\mathsf{d}t$ and h^{-1} is the inverse function of h; *i.e.*, if $h(t) = \lambda_2$ then $h^{-1}(\lambda_2) = t$.

The pressure for the SURFplus model is determined by subtracting out the carbon cluster energy from the equilibrium EOS; *i.e.*,

$$\widetilde{P}(V, e, \lambda, \lambda_2) = P(V, e - \lambda \, e_{CC}(\lambda_2), \lambda) \ , \tag{B.4}$$

where $P(V, e, \lambda)$ is the mixture EOS for the SURF model.

C PBX 9502 EOS model

The Davis EOS is used for the HE; see Wescott et al. [2005] and references therein. Both reactants and products EOS have the Mie-Grüneisen form for the pressure,

$$P(V,e) = P_{\text{ref}}(V) + \frac{\Gamma(V)}{V}\Big[e - e_{\text{ref}}(V)\Big] \ , \tag{C.1}$$

with an isentrope for the reference curve; $e_{\text{ref}}(V) = e_0 - \int_{V_0}^{V} \mathrm{d}V\, P_{\text{ref}}(V)$. The products EOS utilizes a constant specific heat. Hence,

$$T(V,e) = T_{\text{ref}}(V) + \Big[e - e_{\text{ref}}(V)\Big]/C_v \ , \tag{C.2a}$$

$$T_{\text{ref}}(V) = T_0 \exp\Big[-\int_{V_0}^{V} \mathrm{d}V\, \Gamma(V)/V\Big] \ . \tag{C.2b}$$

The reactants EOS has a specific heat linear in entropy. Both EOS are thermodynamically consistent.

Parameters calibrated to PBX 9502 are given in table 1. Based on the EOS model, the calculated CJ detonation state is listed in table 2. The Hugoniot and detonation loci are shown in fig. 21.

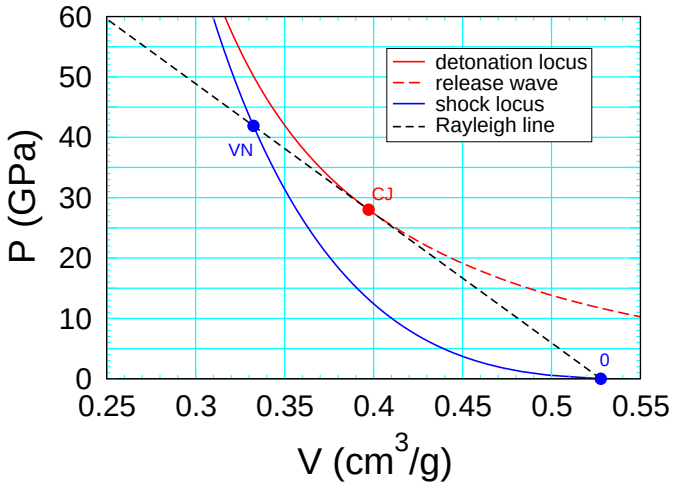

Figure 21: Shock and detonation loci for PBX 9502 based on the Davis EOS.

Table 1: Davis EOS parameters for PBX 9502 from Wescott et al. [2005].

Reactants

V_0 cc/g	e_0 MJ/kg	P_0 GPa	T_0 K	A mm/μs	B –	C –	Γ_0 –	Z –	$C_{v,0}$ MJ/kg·K	α –
0.527704	0.0001	0.0	293	1.75	5.2	0.1	0.8168	0.3093	0.000979	0.7331

Products

ρ_0 g/cc	e_0 MJ/kg	a –	n –	b –	k –	C_v MJ/kg·K	V_c cc/g	p_c GPa	e_c MJ/kg	T_c K
1.895	3.731	0.8592	2.521	0.58	1.3	0.000725	0.9884	1.307	1.1144	1782.6

Table 2: CJ detonation state for PBX 9502 based on model EOS.

	V cm^3/g	e MJ/kg	P GPa	T K	u_p km/s	c km/s
Init state	0.5277	0.0	0.0001	296	0.0	1.75
detonation speed 7.73 km/s						
VN spike	0.3325	4.089	41.9	1631	2.86	7.79
CJ state	0.3972	1.827	28.0	3083	1.91	5.82

For completeness, the functional forms for the Davis EOS are as follows.

Reactants EOS

$$P_{\text{ref}}(V) = P_0 + p_s \left[y_b + \tfrac{1}{2}\, y_b^2 + \tfrac{1}{6}\, y_b^3 + \tfrac{1}{24}\, C\, y_b^4 + y^2\, v^4 \right] , \tag{C.3a}$$

$$e_{\text{ref}}(V) = e_0 + P_0\,(V_0 - V) + p_s\, V_0 \left[\tfrac{1}{2}\, y\, (y_b + \tfrac{1}{3} y_b^2 + \tfrac{1}{12} y_b^4 + \tfrac{1}{60} C\, y_b^5) + v - v^2 + \tfrac{1}{3}(v^3 - 1) \right] , \tag{C.3b}$$

$$\Gamma(V) = \Gamma_0 + Z\, y \ , \tag{C.3c}$$

$$T_{\text{ref}}(V) = T_0 \exp[-Z\, y]\, v^{(\Gamma_0 + Z)} \ , \tag{C.3d}$$

$$T(V, e) = T_{\text{ref}}(V) \left[1 + (1 + \alpha)\, \frac{e - e_{\text{ref}}(V)}{C_{v,0}\, T_{\text{ref}}(V)} \right]^{\frac{1}{1+\alpha}} \ , \tag{C.3e}$$

where

$$v = V_0/V \ , \tag{C.3f}$$
$$y = 1 - V/V_0 \ , \tag{C.3g}$$
$$y_b = 4\,B\,y \ , \tag{C.3h}$$
$$p_s = A^2(4\,B\,V_0)^{-1} \ . \tag{C.3i}$$

The EOS domain is limited in expansion, $V > V_0$, when either the isothermal bulk modulus or $\Gamma(V)$ goes negative.

Products EOS

$$P_{\rm ref}(V) = p_c\,\frac{k-1+f(v)}{k-1+a}\left[\tfrac{1}{2}(v^n+v^{-n})\right]^{a/n} v^{-(k+a)} \ , \tag{C.4a}$$
$$e_{\rm ref}(V) = e_c\left[\tfrac{1}{2}(v^n+v^{-n})\right]^{a/n} v^{-(k-1+a)} - e_0 \ , \tag{C.4b}$$
$$\Gamma(V) = (k-1) + (1-b)\,f(v) \ , \tag{C.4c}$$
$$T_{\rm ref}(V) = T_c\left[\tfrac{1}{2}(v^n+v^{-n})\right]^{[a\,(1-b)/n]} v^{-[k-1+a(1-b)]} \ , \tag{C.4d}$$

where

$$v = V/V_c \ , \tag{C.4e}$$
$$f(v) = \frac{2\,a}{1+v^{2n}} \ , \tag{C.4f}$$
$$e_c = p_c\,V_c/(k-1+a) \ , \tag{C.4g}$$
$$T_c = \frac{2^{-a\,b/n}}{k-1+a}\,\frac{p_c\,Vc}{C_v} \ . \tag{C.4h}$$

D SURF burn parameters

The current fitting form for the reactive strength function $f(P_s)$ has 5 dimensionless parameters, p_0, p_1, A, B, df_1, and 2 parameters to set the scales for pressure and time, P_{ref} and t_{ref};

$$f(P_s) = t_{ref}^{-1} \begin{cases} 0, & \text{for} \quad p_s \le p_0 \\ f_0(p_s) - f_0(p_0)\left[1 + B\,(p_s - p_0)\right], & \text{for } p_0 < p_s \le p_1 \\ f_1\left[1 + df_1\left(1 - \exp\left[-B_2\,(p_s - p_1)\right]\right)\right], & \text{for } p_1 < p_s \end{cases} \tag{D.1a}$$

where

$$p_s = P_s / P_{ref} \tag{D.1b}$$

$$f_0(p_s) = \exp(A + B\,p_s)\ , \tag{D.1c}$$

$$f_1 = f_0(p_1) - f_0(p_0)\left[1 + B\,(p_1 - p_0)\right]\ , \tag{D.1d}$$

$$B_2 = \frac{B}{df_1} \cdot \frac{f_0(p_1) - f_0(p_0)}{f_1}\ . \tag{D.1e}$$

By construction f and $\mathsf{d}f/\mathsf{d}P_s$ are continuous at $p_0\,P_{ref}$ and $p_1\,P_{ref}$, and $f(P_s)$ asymptotes to a finite value, $f_1 \cdot (1 + df_1)$, for large P_s.

Illustrative SURF parameters for PBX 9502 and a plot of $\log f(P_s)$ vs $\log P_s$ are shown in fig. 22. In the region that dominates shock initiation, the linear portion of the curve implies that $f(P_s)$ is approximately proportional to a power of P_s. The cutoff at large P_s affects the reaction zone width of a propagating detonation wave, and hence the curvature effect; *i.e.*, detonation speed as a function of front curvature. The cutoff at low pressure leads to a threshold pressure for shock initiation; *i.e.*, cuts off the Pop plot for weak shocks.

The reaction scale function $g(s)$ is defined by

$$g(s) = [g_{scale}]^{-1} \times \begin{cases} g_0(s)\ , & \text{for } s \le s_1 \\ g_0(s_1) + g_0'(s_1)\,(s - s_1) + \frac{1}{2}\,g_0''(s_1)\,(s - s_1)^2\ , & \text{for } s_1 < s \le s_{max} \end{cases} \tag{D.2a}$$

where s_1 is a parameter and

$$g_0(s) = \exp(-s^2)\ , \tag{D.2b}$$

$$g_{scale} = g_0(s_1) - \tfrac{1}{2}\,[g_0'(s_1)]^2 / g_0''(s_1)\ , \tag{D.2c}$$

$$s_{max} = s_1 - g_0'(s_1)/g_0''(s_1)\ . \tag{D.2d}$$

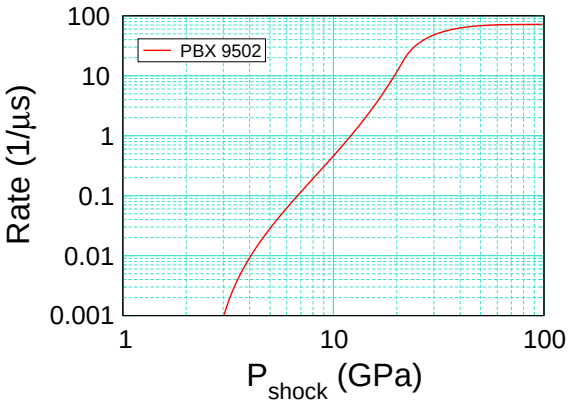

parameters

P_{ref}	1 GPa
t_{ref}	1 μs
p_0	2.5
p_1	21.5
A	-3.1
B	0.28
df_1	3.0

Figure 22: SURF rate for PBX 9502.

By construction, $g(s)$ and its first two derivatives are continuous at the transition point s_1. Moreover, $g(s_{max}) = 1$ and $g'(s_{max}) = 0$. Consequently, a detonation wave has a finite reaction zone width and the rate goes smoothly to zero at the end of the reaction zone. The function $g(s)$ for $s_1 = 2$ is shown in fig. 23. For this case, $s_{max} = 2.286$. We note that the burn rate,

$$\mathsf{d}\lambda/\mathsf{d}t = (\mathsf{d}g/\mathsf{d}s)(\mathsf{d}s/\mathsf{d}t) \ , \tag{D.3}$$

is 0 at the shock front since $\mathsf{d}g/\mathsf{d}s = 0$ at $s = 0$. Also, for $n = 0$ (no pressure dependence in the rate), the reaction time is given by $s_{max}/f(P_s)$.

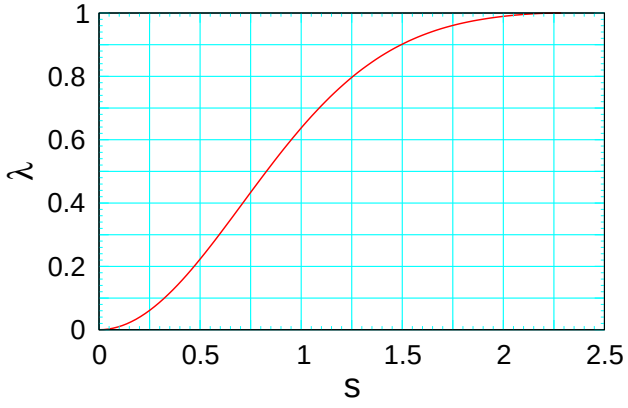

Figure 23: Reaction scale function with $s_1 = 2$.

D.1 SURFplus extension

The limiting carbon cluster reaction function is defined by 4 parameters: t_1 and t_2 with dimensions of time, and dimensionless parameters h_1 and h_2. The fitting form is

$$h(t) = \begin{cases} \frac{1}{2}\, a_1\, t^2 \ , & \text{for } t_0 < t < t_1 \\ h_1 + [(h_2 - h_1)/(t_2 - t_1)]\, (t - t_1) \ , & \text{for } t_1 < t < t_2 \\ 1 - \frac{1}{2}\, a_3\, (t_3 - t)^2 \ , & \text{for } t_2 < t < t_3 \end{cases} \tag{D.4}$$

where

$$a_2 = (h_2 - h_1)/(t_2 - t_1) \tag{D.5a}$$

$$t_0 = t_1 - 2\, h_1/a_2 \tag{D.5b}$$

$$a_1 = 0.5\, a_2^2/h_1 \tag{D.5c}$$

$$t_3 = t_2 + 2\, (1 - h_2)/a_2 \tag{D.5d}$$

$$a_3 = 0.5\, a_2^2/(1 - h_2) \tag{D.5e}$$

Illustrative parameters for PBX 9502 and a plot of $h(t)$ are shown in fig. 24. By construction, $h(t)$ is linear in the range between h_1 and h_2.

We note that $h'(0) = 0$. Therefore, $\lambda_2 = 0$ is a fixed point of Eq. (B.3). To get around this, we express $\lambda_2 = s_2^2$. The transformed rate equation for s_2,

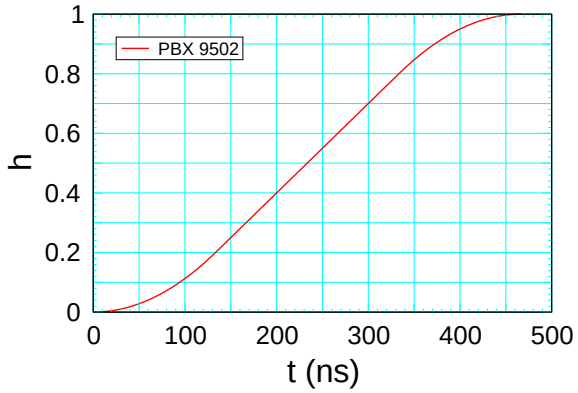

parameters	
t_1	$0.150\,\mu$s
h_1	0.2
t_2	$0.350\,\mu$s
h_2	0.8

Figure 24: Limiting carbon cluster reaction function for SURFplus model of PBX 9502.

$$\frac{\mathrm{d}}{\mathrm{d}t}s_2 = \tfrac{1}{2}\lambda^2 \begin{cases} \frac{h_1 a_2}{h_1 s_2 + (t_1 a_2 - h_1)(h_1^{1/2} - s_2)} \ , & \text{for } s_2^2 < h_1 \ ; \\ a_2/s_2 \ , & \text{for } h_1 \le s_2^2 \le h_2 \ ; \\ [2(1-s_2^2)\, a_3]^{1/2}/s_2 \ , & \text{for } h_2 < s_2^2 \ ; \end{cases} \tag{D.6}$$

is then regular at the start of the carbon clustering reaction.

A plot of the carbon cluster energy B.2 and parameters are shown in fig. 25. The detonation loci with and without the carbon cluster energy corresponds to the Hugoniot loci with pressures $P_{prod}\big(V, e\big)$ and $P_{prod}\big(V, e - e_{CC}(0)\big)$, respectively. In effect, the locus without carbon clustering corresponds to using the products EOS with a negative heat release; $-e_{CC}(0)$. Plots of these loci are shown in fig. 26. Due to the effective negative energy release, the locus without carbon clustering lies below the locus with carbon clustering. The CJ state without the carbon cluster energy is listed in table 3. Compared to the CJ state with the carbon clustering energy, table 2, the detonation speed is lower by 4.7% and the CJ pressure is lower by 11%.

For the CJ detonation wave of the SURFplus model, the state at the end of the fast SURF reaction corresponds to the state on the overdriven detonation locus without the carbon clustering at the CJ detonation speed of the full reaction, which has a pressure of 37.4 GPa.

Other reactive burn model, such as the three term Ignition & Growth model [Tarver et al., 1985], have fast and slow rate terms with a single reaction. At a specified value of the reaction progress variable, λ_c, the rate switches. In effect, the first fast reaction corresponds to $0 \le \lambda < \lambda_c$, and the second slow reaction corresponds to $\lambda_c < \lambda \le 1$. Qualitatively, the effect is similar to the two reactions in the SURFplus model. The analog of the detonation loci with

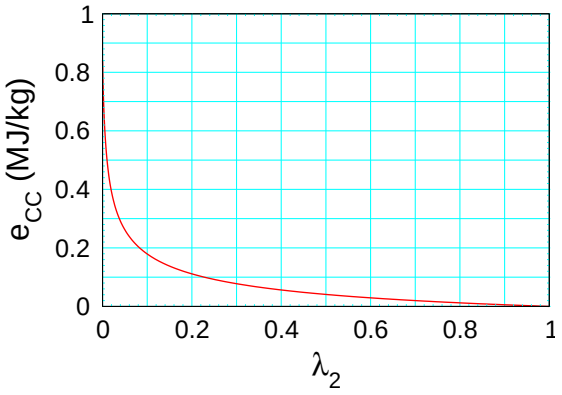

parameters	
Q	1. MJ/kg
N_{ratio}	250.

Figure 25: Carbon-clustering energy for SURFplus model of PBX 9502.

and without carbon clustering are the fully burned detonation locus and the partly burned locus with burn fraction λ_c. Geometrically, the loci are similar to those shown in fig. 26.

Table 3: CJ detonation state for PBX 9502 based on model EOS without carbon cluster energy.

	V cm^3/g	e MJ/kg	P GPa	T K	u_p km/s	c km/s
Init state	0.5277	0.0	0.0001	296	0.0	1.75
detonation speed 7.37 km/s						
VN spike	0.3413	3.384	36.3	1439	2.86	7.60
CJ state	0.4005	1.577	24.8	2686	1.78	5.59

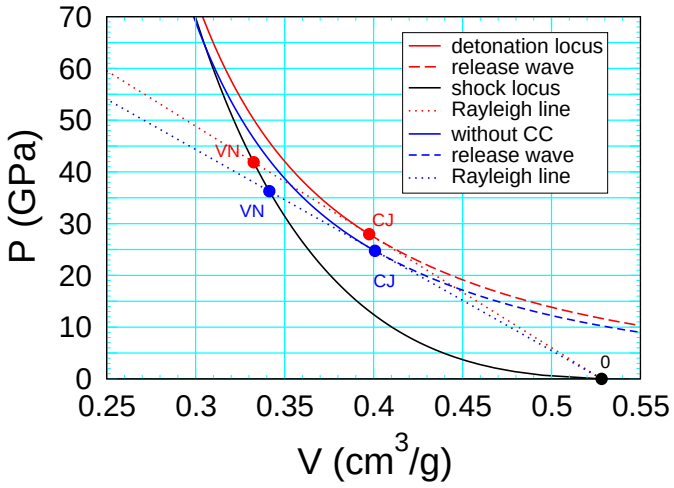

Figure 26: Shock and detonation loci with and without energy release from carbon clustering.

References

W. Fickett and W. C. Davis. *Detonation*. Univ. of Calif. Press, 1979. 2

E. L. Lee and C. M. Tarver. Phenomenological model of shock initiation in heterogeneous explosives. *Phys. Fluids*, 23:2362–272, 1980. 2

R. Menikoff. Detonation wave profile. Technical Report LA-UR-15-29498, Los Alamos National Lab., 2015. 17

R. Menikoff and M. S. Shaw. Reactive burn models and ignition & growth concept. *EPJ Web of Conferences*, 10, 2010. doi: 10.1051/epjconf/20101000003. URL http://www.epj-conferences.org/articles/epjconf/pdf/2010/09/epjconf_nmh2010_00003.pdf. 2

M. S. Shaw and R. Menikoff. Reactive burn model for shock initiation in a PBX: Scaling and separability based on the hot spot concept. In *Fourteenth Symposium (International) on Detonation*, 2010. 2

C. M. Tarver, J. O. Hallquist, and L. M. Erickson. Modeling short pulse duration shock initiation of solid explosives. In *Eighth Symposium (International) on Detonation*, pages 951–961, 1985. 27

B. L. Wescott, D. S. Stewart, and W. C. Davis. Equation of state and reaction rate for condensed-phase explosives. *Journal of Applied Physics*, 98:053514, 2005. 12, 21, 22